# Radar - Rainfall Infilling Techniques

**S. M. Wesson, G.G.S Pegram**

Civil Engineering, University of KwaZulu-Natal, DURBAN, 4014

## Abstract

A technique has been developed to estimate all the unknown data in a radar volume scan. The technique is computationally fast and works on a real time basis; it comprises the following steps. A correction algorithm is employed to adjust reflectivity values affected by the bright band. A rainfall classification algorithm is then applied to separate the rainfall into two separate types: convective and stratiform. Climatological semivariograms based on the rainfall type are then defined.

All missing data in the radar volume scan are then estimated using 3D Universal and/or Ordinary Cascade Kriging; computational efficiency and stability in Kriging are ensured by using a nearest neighbours approach and a Singular Value Decomposition (SVD) matrix rank reduction technique. To validate the proposed method, a statistical comparison is carried out for selected rain events, comparing (i) the radar accumulation estimates at ground level with (ii) raingauge accumulations over a dense raingauge network calculated by Block Kriging.

***Keywords:*** *bright band adjustment, rainfall classification, climatological semivariograms, Kriging.*

## 1 Introduction

Currently in South Africa the weather radar network of 11 C-band radars provides images of the instantaneous reflectivity values at approximately five-minute intervals and at a one-kilometre horizontal resolution supplied in Cartesian co-ordinates on Constant Altitude Plan Position Indicators (CAPPI's) at 1km intervals above ground level. This type of data provides a detailed spatial representation of the rainfield in real time and over a large area

Rainfields estimated from weather radars experience various data quality problems such as ground clutter, anomalous propagation and beam blocking to name a few (Terblanche et al, 2001). Another disadvantage of weather radars is that they provide an indirect measurement of the rainfall, so the returned power of measured reflectivity values has be converted to rainrate by an appropriate transformation, such as, the Marshall Palmer formula (Marshall and Palmer, 1948). Figure 1 illustrates a typical instantaneous radar reflectivity image taken from the Bethlehem (South Africa) S-band weather radar where the white portions indicate no rainfall, grey portions indicate areas out of the weather radar's range and also where there are no data available, and the black regions mark ground clutter locations.

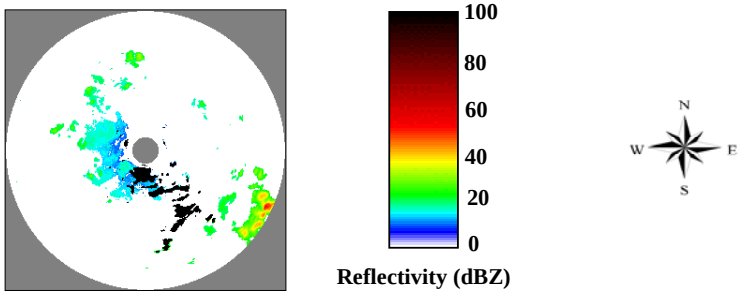


**Figure 1. Typical radar reflectivity image taken from the Bethlehem (South Africa) weather radar on the 25 February 2003. The grey portions of the image indicate where no data are available and the black regions indicate ground clutter. The image is 300km square.**

The data in the CAPPIs are only available from one-kilometre above ground level and regions within the volume scan exist where the rainrate is unknown. In applications, such as disaster management, hydrology and agriculture, the rainfall estimates at ground level are of more interest and importance than the measurements aloft. The data aloft are unlikely to be an accurate indication of the rainfall at ground level (Jordan et al, 2000) since the precipitation tends to be affected by a variety of atmospheric phenomena before reaching the earth's surface.

This paper presents a technique to extrapolate radar data contained aloft in the radar volume scan to ground level in the process estimating all unknown data. Firstly the details of the rainfall classification algorithm are outlined and the characteristics of the classified rainfall described. The next part describes the empirical computation of the Robust semivariogram from radar reflectivity data and outlines the use and validation of climatalogical semivariograms based on rainfall type. Kriging theory is then discussed where the methods designed to ensure computational efficiency and stability are outlined. 3D Universal and Ordinary Kriging are then discussed in their application to Cascade Kriging, a novel idea for extrapolation. Finally a statistical comparison between the temporally accumulated radar estimates and the Block Kriged rainguage estimates is carried out over matching areas to determine the quality of the rainfall estimates at ground level.

## 2 Rainfall Classification

The initial step of the operational algorithm for infilling the missing or inaccurate data on a CAPPI requires a simple classification and thresholding of the instantaneous radar volume scan data, pixel by pixel. The algorithm developed here, with assistance of meteorologists from METSYS (Meteorological Systems and Technology - a research division of the South African Weather Service), classifies the rainfall into two groups: convective and stratiform, like Steiner's (1995) algorithm, and works as follows. The classification is done pixel by pixel throughout the volume scan data. The initial step of the algorithm works on a simple threshold where all reflectivity values less than or equal to 18dBZ are set to zero due to the fact that 18dBZ approximates to 0.50 mm/hr, a rate that can be considered negligible. The remainder of the reflectivity values above zero are then classified by the simple criterion: if the reflectivity value is 35dBZ or above, the rainfall is classified as convective; the reflectivity values in the range 18dBZ to 35dBZ are classified as stratiform rainfall. A summary of the classification criteria are contained in Table 1.

**Table 1. Rainfall classification and threshold criteria to separate radar volume scan data into stratiform and convective rainfall domains.**

| CRITERIA | CLASSIFICATION |
|---|---|
| Pixel ≤ 18 dBZ | No Rainfall: Pixel set to 0 dBZ |
| 18 dBZ < Pixel < 35 dBZ | Stratiform Rain |
| Pixel ≥ 35 dBZ | Convective Rain |

The advantages of this algorithm are its simplicity and effectiveness, in that for a real time application it has little impact on the overall computation time; this is especially true for large data sets such as those returned from weather radar volume scans. An example of an instantaneous reflectivity image that has been classified is indicated by Figure 2. The image is taken from the Bethlehem weather radar (30 December 2001) from the 4km CAPPI level; the left hand side image indicates the instantaneous reflectivity image and the left hand side image the classified rainfall.

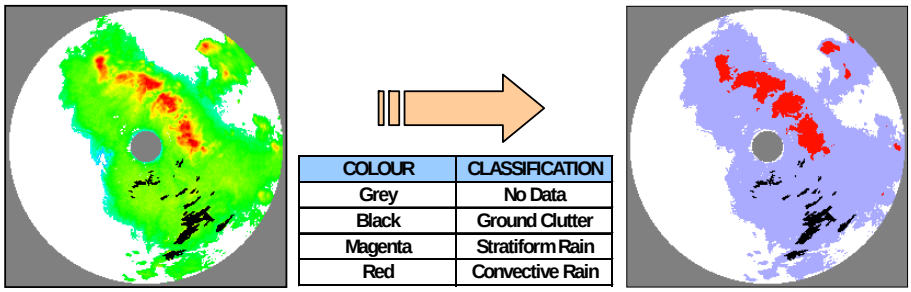


**Figure 2. Radar reflectivity image from the Bethlehem weather radar (30 December 2001) and the corresponding classified image. Each image is 300km square.**

### 2.1 Characteristics of Classified Rainfall

The vertical characteristics of the classified stratiform and convective rain were examined by computing the mean vertical profile of reflectivity from selected images from the Durban and Bethlehem weather radars over five different years (1995, 1996, 2000, 2001 and 2002). As shown in Figure 3 the stratiform rain generally has a low average vertical height, limited to 8km above ground level. The convective rainfall has considerable vertical extent ranging up to 14km above ground level and a bigger range in mean reflectivity values. Both the stratiform and convective profiles show a constant increase in rainfall intensity as ground level is approached, with the exception that in the stratiform profile, evidence of a bright band at the 2km level indicates that the stratiform rain has been classified correctly. The variability of the reflectivity in both are characterised by a standard deviation of 3.5dB or less at any level.

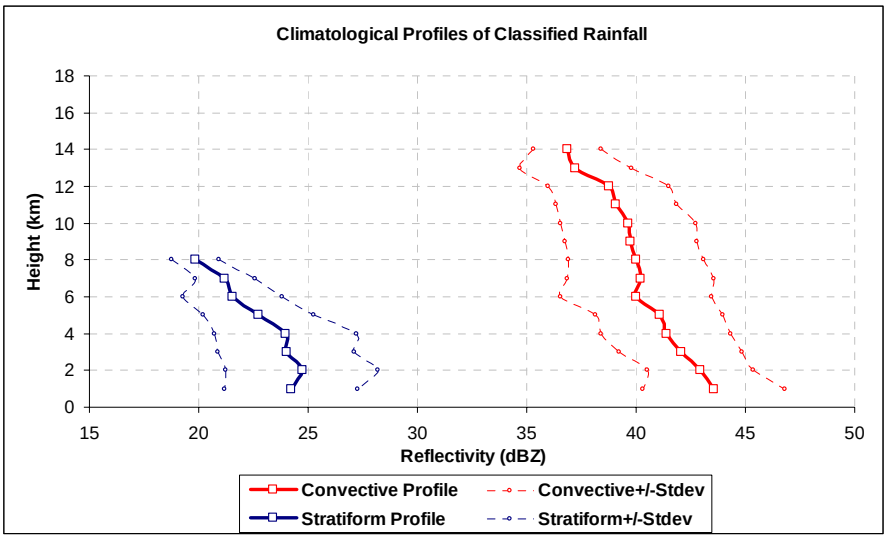


**Figure 3. Average vertical profile of reflectivity for classified stratiform and convective rainfall. Profiles are computed from 20 different images ranging over a 5 year period from the Bethlehem and Durban weather radars.**

## 3 Bright Band Adjustment

As snow and ice crystals drop through the 0°C isotherm they begin to melt and are surrounded by a thin layer of water. The result is that the melting snow and ice crystals resemble large blobs of water and the reflectivity values for the melting level are enhanced greatly providing an overestimation of rain (Sanchez-Diezma et al, 2000). This level is called the bright band. At Bethlehem, South Africa the bright band generally occurs 2km above ground level (Mittermaier, 1999) as can be seen by the stratiform climatological profile of reflectivity in Figure 3.

The presence of a bright band has an adverse effect on the estimates at ground level when applying an extrapolation algorithm to volume scan radar reflectivity data. When extrapolating to a target point at ground level the control points are selected from the 1km and 2km CAPPI levels; the trend of decreasing reflectivity is then extrapolated to ground level resulting in lower estimates of stratiform rainfall than should be expected.

The first step of the algorithm computes the wetted area ratio (WAR) of stratiform rainfall on the 3km, 2km and 1km CAPPI levels. If the WAR of stratiform rainfall is less than 10% on any of the CAPPI levels then no correction takes place due to insufficient rainfall to determine if a bright band is present; if the WAR of stratiform rainfall is greater than 10% the 2km CAPPI level is then examined for evidence of a bright band. The existence of the bright band is determined by comparing the mean value of reflectivity on the 1km, 2km and 3km ( $\bar{x}_1$, $\bar{x}_2$ and $\bar{x}_3$) CAPPI levels of the reflectivity values classified as stratiform rainfall. If the computed mean values of the stratiform rainfall are $\bar{x}_1 > \bar{x}_3$ and $\bar{x}_2 \geq \bar{x}_1$ then a bright band is considered to be present in that vertical reflectivity profile. Some memory of the mean value from the previous time step is retained by geometric weighting.

If a bright band is identified, all the values classified as stratiform rainfall are then evaluated on an individual pixel by pixel basis, to identify if the individual pixel point on the 2km CAPPI is affected by the bright band. For each stratiform pixel location on the 2km CAPPI level the gradient ($\Delta_{critical}$ = ΔdBZ/Δheight) is calculated between the pixel value (contained directly above it) on the 3km CAPPI and the value equal to $x_1+\sigma_1$ on the 1km CAPPI level. The gradient ($\Delta_{observed}$) is also calculated between the pixel on the 3 km and 2km CAPPI level.

If the absolute values of $\Delta_{observed} \geq \Delta_{critical}$ then the pixel on the 2km CAPPI level is classified as a bright band point and adjusted by altering the value of that point as shown in Equation (1).

$$New\ dBZ_2\ Pixel = \frac{dBZ_3 + \bar{x}_1}{2} \tag{1}$$

To test the effectiveness of the proposed bright band correction procedure a period of rainfall from the Bethlehem weather radar was selected (17 December 1995) that consisted predominantly of stratiform rainfall and showed clear evidence of a bright band. Figure 4 illustrates the computed mean values of CAPPI levels 1, 2 and 3 throughout the day. The mean value of CAPPI 2 (green line with triangle markers) is consistently higher throughout the day than the mean values on the 1km and 3km CAPPI levels illustrating a clear bright band.

The bright band correction procedure described was applied to each instantaneous image throughout the 24 hour period. The mean value of the adjusted reflectivity data on the 2km CAPPI level was then recomputed. Figure 4 illustrates the adjusted mean value for the 2km CAPPI level, which now lies at the approximate midpoint of the mean value for the 1km and 3km CAPPI level. The results indicate a successful adjustment of the pixels affected by bright band on the 2km CAPPI level.

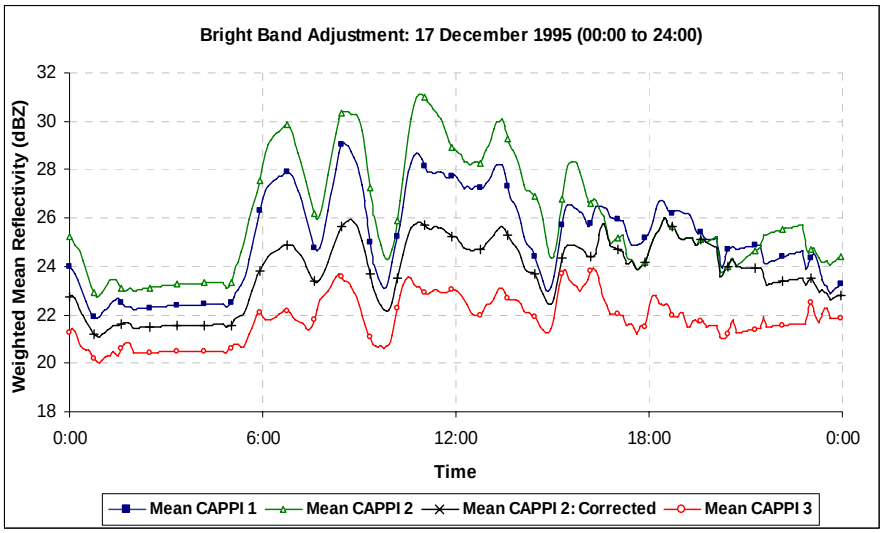


**Figure 4. Bright band adjustment of the 2km CAPPI level for the 17 December 1995 (00:00 to 24:00). The green line with triangle markers indicates the 2km CAPPI level affected by bright band and the black line with plus sign markers indicates the mean value of the corrected data on the 2km CAPPI level.**

## 4 Semivariogram Estimation

The semivariogram provides a way of measuring the spatial dependence that exists amongst the variables in a stationary random field. The Kriging computation can be carried out using either a covariance or a semivariogram function. However in this application the semivariogram is used in preference due to its more robust properties as outlined by Cressie (1993: 70-73).

The semivariogram is most commonly computed by the Classical Variogram estimator as was proposed by Matherhon (1962). Unfortunately the classical estimator is badly affected by non-typical observations (Cressie, 1993: 40). The effect of non-typical data points can have a dramatic effect on the semivariogram since they are used numerous times in the calculation at different lag intervals. This can result in peaks or shifting of the entire semivariogram upwards (Sabyasachi et al, 1997).

It was thus decided that the Robust Variogram, proposed by Cressie and Hawkins (1980) was the more appropriate model to use and is given by Equation (2).

$$2\cdot\bar{\gamma}(h)=\left\{\frac{1}{|N(h)|}\sum_{N(h)}\left|Z(s_i)-Z(s_j)\right|^{1/2}\right\}^4 \Bigg/ \left(0.457+\frac{0.494}{|N(h)|}\right) \tag{2}$$

Where $\bar{\gamma}(h)$ is the sample semivariogram at lag $h$ (the specified lag distance), $Z(s_i)$ and $Z(s_j)$ are the values of the variables at the specified locations, $s_i$ and $s_j$ which are $h$ apart and $N(h)$ is the number of pairs separated by lag $h$. Computing the difference of $Z(s_i)$ and $Z(s_j)$ in the square root domain dramatically decreases the influence of uncharacteristic observations. The two parameter isotropic model is then chosen to fit the empirical semivariogram values, as defined by Equation (3).

$$g(h)=1-\exp[-(h/L)^{\alpha}] \tag{3}$$

Where $h$ is the Euclidian distance between points, $L$ the correlation length and $\alpha$ the shape parameter which lies in the range $0<\alpha\leq 2$. An example of a semivariogram is shown in Figure 5, computed from a 30km square section of radar reflectivity data selected from the Durban weather radar (11 December 2000). The data are initially standardised to produce a scaled and dimensionless field. In this instance the correlation length $L$ = 8.31km and the shape parameter $\alpha$ = 1.38.

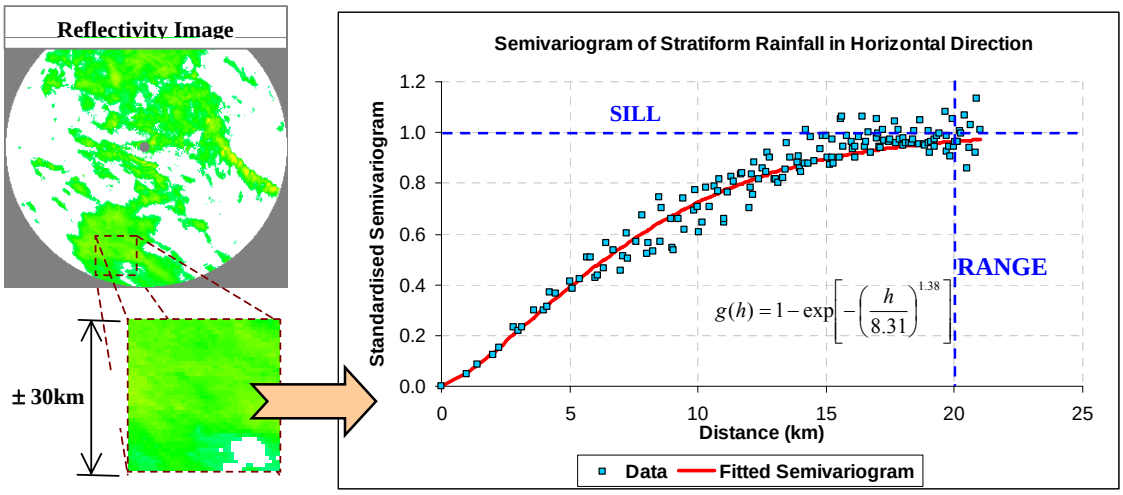


**Figure 5. Typical semivariogram computed from a selected portion of stratiform rain with the sill and approximate range indicated. The maximum distance between pixels ($d_{max}$) is 42km, so *h* is limited to half of that (21km) as recommended by Journel and Huijbrechts (1978: 194).**

## 4.1 Parameter Fitting to Rainfall Type

To compute the semivariogram parameters ($\alpha$ and $L$), each time an unknown reflectivity value needs to be estimated, is time consuming and not a realistic option for a real time application. An alternative is therefore needed that is computational efficient yet does not compromise the accuracy of the results. The concept of employing climatological semivariograms based on the type of classified rainfall was explored.

The rainfall classification algorithm, described in Section 2, was applied to a set of instantaneous reflectivity images selected from the Bethlehem and Durban weather radars over a period of several years (1995, 2000, 2001 and 2002). From these images, regions were selected with areas approximately 1200km$^2$ (40km by 30km) or larger. From the regions selected, the Robust semivariogram was computed (Equation 2) and the two parameter exponential model (Equation 3) fitted. This was done in both the horizontal and vertical direction. The two parameters were then plotted against one another in a scatter plot; as indicated by Figure 6 for the horizontal direction and vertical direction. The scatter plots in Figure 6 illustrate that the semivariogram parameters tend to cluster in a particular region according to the rainfall type, indicating that a fixed set of parameters might be used, depending on rainfall type.

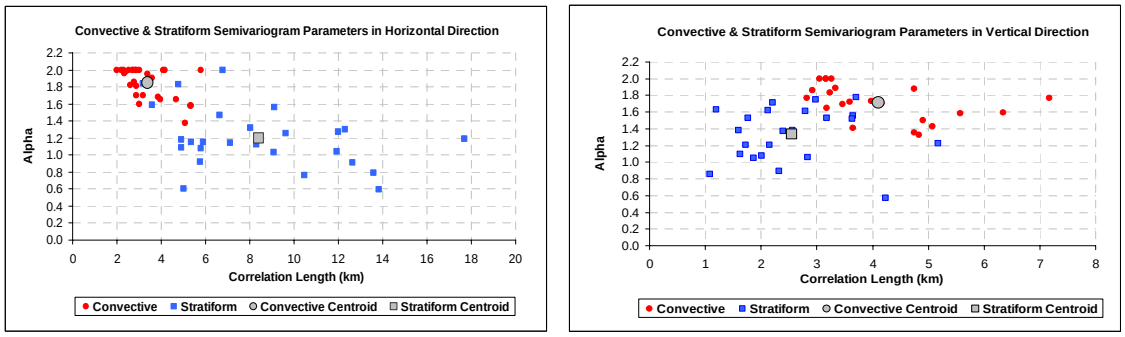


**Figure 6. Scatter plots of alpha ($\alpha$) and correlation length ($L$) parameters for stratiform and convective rainfall in the horizontal and vertical direction.**

### 4.2 Cluster and Sensitivity Analysis

To test if a natural clustering of the variables occurs, a Fuzzy C-Means clustering algorithm (Gordon, 1981: 58-60) was run on a scatter plot of the data, where the specification set in the algorithm was that the data should be divided into two groups. In the horizontal direction the cluster algorithm roughly split the two groups along the 6.5km correlation length and 24% of the points were misclassified. In the vertical direction the cluster algorithm roughly split the two groups along the 3.5km correlation length and 30% of the points were misclassified. This indicates a natural separation of the parameters into two groups in the horizontal and vertical directions depending on rainfall type.

To determine how sensitive the final Kriged solutions are, to the use of a fixed set of semivariogram parameters, a sensitivity analysis was undertaken. 2D data sets of reflectivity were selected containing solely convective or stratiform rainfall. Portions were removed and Ordinary Kriging used to estimate the missing data. In this instance the data were infilled several times using different combinations of semivariogram parameters. Five different combinations were used: firstly the centroid value of $\alpha$ and $L$ for convective and stratiform rain and then the $\alpha$ and $L$ values one standard deviation away from the centroid values.

The infilled data were then compared to the original observed reflectivity data by computing the sum of the differences squared, the means and standard deviations of the observed and estimated data. The results indicate that there is no significant difference between the five sets of parameter values used in each instance, giving a clear indication that the final Kriged solution is reasonably insensitive to the range of the shape parameter ($\alpha$) and correlation length ($L$) values that can possibly occur when a sample semivariogram is fitted to a specific rainfall type. Instead of solving for each set of semivariogram parameters for each neighbourhood, one can simply use the centroid value computed for each rainfall type depending on the observed rainfall. The fixed set of semivariogram parameters can therefore be used in the Kriging process in the horizontal and vertical direction for convective and stratiform rainfall. The parameters are indicated in Table 2.

**Table 2. Semivariogram parameter values in the horizontal and vertical directions for stratiform and convective rainfall.**

| | HORIZONTAL | | VERTICAL | |
|---|---|---|---|---|
| | $\alpha_H$ | $L_H$ (km) | $\alpha_V$ | $L_V$ (km) |
| **STRATIFORM** | 1.53 | 8.40 | 1.33 | 2.56 |
| **CONVECTIVE** | 1.85 | 3.38 | 1.71 | 4.11 |

## 5 Kriging Methods

Kriging was chosen as the computational method to interpolate the observations missing internal to the CAPPI stack and to extrapolate the reflectivity values contained aloft to ground level. Kriging is considered to be the optimal technique for the spatial prediction of Gaussian data (Cressie, 1993: 106). In Ordinary Kriging, the mean is assumed constant and unknown throughout the field whereas in Universal Kriging, the mean is also assumed to be unknown but varying (Chiles and Delfiner, 1999: 151). The Ordinary Kriging equation is given by Equation (4):

$$z(s_0) = \lambda^T(s_0) \cdot z \tag{4}$$

Here $z(s_0)$ is the value to be estimated at the target point $s_0$, $z$ is the vector of known reflectivity values, or control points, and the row vector $\lambda^T(s_0)$ contains the calculated weighting values which depend on $s_0$. The weighting values contained in the vector $\lambda^T(s_0)$ are computed by Equation (5).

$$\begin{bmatrix} G & u \\ u^T & 0 \end{bmatrix} \cdot \begin{bmatrix} \lambda(s_0) \\ \mu(s_0) \end{bmatrix} = \begin{bmatrix} g(s_0) \\ 1 \end{bmatrix} \tag{5}$$

Where $G$ is a matrix of semivariogram values between the control points, $u$ a unit vector of ones, $\lambda(s_0)$ the vector of weighting values, $\mu(s_0)$ a Lagrange multiplier and $g(s_0)$ a vector of semivariogram values between the target point at $s_o$ and control point locations.

In Universal Kriging external variables can be added to the coefficient matrix that model the variation of the mean in the field. It was determined that in the mixed zone, where the control points consist of convective and stratiform pixels, Universal Kriging provided an improved estimate over Ordinary Kriging. A stratiform/convective binary switch was used as the two external variables in Universal Kriging, where $C$ represents a convective and $S$ a stratiform control point, so that a convective control point is assigned the values $[C\ S] = [1\ 0]$ and a stratiform control point is assigned the values $[C\ S] = [0\ 1]$. In situations where the control points consisted of either purely stratiform or convective pixels Ordinary, not Universal Kriging is used to estimate the target point.

## 5.1 Computational Stability and Efficiency

Computational efficiency is ensured by using neighbourhood Kriging to estimate each target value individually, where in this application the computed optimum number of control points based on an exhaustive comparison, is 25. An unexpected problem associated with the Kriging technique, which is not so well known, is the ill-conditioning of the coefficient matrix. It was demonstrated by Wesson and Pegram (2004) that the coefficient matrix can be highly ill-conditioned dependent on a number of factors, most notably as the alpha parameter in the semivariogram function tends to Gaussian ($\alpha \rightarrow 2$). The method of Singular Value Decomposition (SVD) is therefore used in conjunction with a trimming of the singular values to provide a computational stable method to find the solution to the Kriging equations.

## 5.2 Cascade Kriging

When Kriging directly to ground level using the full set of CAPPI data in a stack, there are unexpected problems which occur. Serious discontinuities at the regions located directly under the edges of the CAPPI levels occur and also inflation of the reflectivity estimates due to the numerical and geometric distribution of Kriging weights occur at the CAPPI edge locations. A solution to the above problem is to use a Cascade Kriging approach. The first step is to infill the missing data in the CAPPI at 4km above ground level, pixel by pixel, using neighbourhood Kriging of the 25 control data vertically above and in the horizontal direction. Once all the unknown data on that CAPPI level have been estimated and infilled, the CAPPI level directly below is examined and any missing data here are estimated in the same manner; once again estimates from above (which now can include previously infilled data) and at the same level are used as control data. This is repeated until all the unknown data from in each CAPPI level are estimated. The final step involves an estimate of the rainfall at ground level.

Figure 7 gives a 3D illustration of radar volume scan data before and after Cascade Kriging. The data are from the Bethlehem weather radar, 14 February 1996, where the image is 200km square, and the vertical extent is 3km. The levels above 3km have been ignored for clarity, but were used to estimate missing data from level 4 downwards. The image on the left hand side indicates the volume scan data before Cascade Kriging and the right hand image represents the same volume scan data after Cascade Kriging has been used to estimate as much unknown data as possible and provide an estimate at ground level.

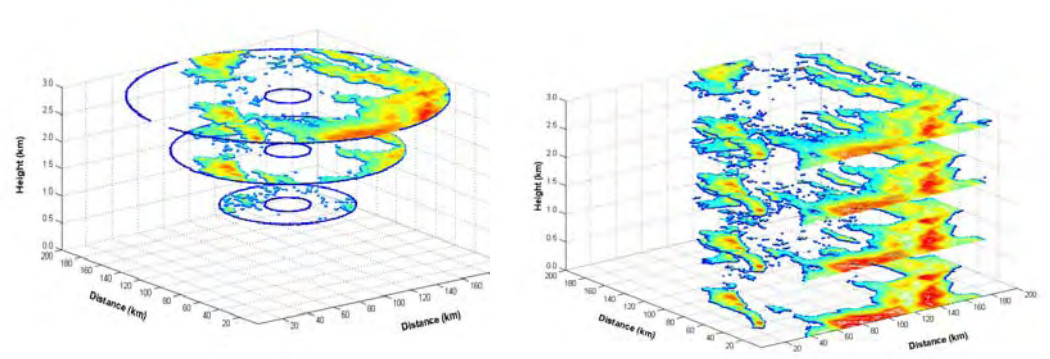


**Figure 7. 3D Graphical illustration of radar volume scan data up to 3km above ground level, before and after Cascade Kriging. Data are from the Bethlehem weather radar (14 February 1996). Data at levels 4, and higher are not shown, but were used to successively fill the stack from above.**

Cascade Kriging has the following influences on reflectivity data. There is increased smoothing and also magnitude of the reflectivity values as ground level is approached, corresponding with the climatological profiles shown in Figure 3. Figure 8 shows an example of the smoothing and the increase in magnitude of the reflectivity values as ground level is approached. The image on the left hand side is at the 4km CAPPI level and the right hand side image indicates the Cascade Kriging estimate at ground level. As can be seen the estimates are smoother and have increased in magnitude.

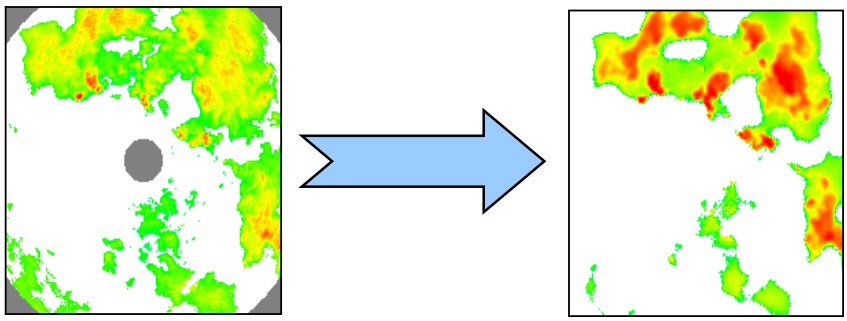

**Observed reflectivity data 4km above ground level**

**Kriged estimate at ground level**

**Figure 8. Example of smoothing and increase in magnitude of the reflectivity values as ground level is approached. The image is from the Bethlehem weather radar from the 25 January 1996, dimensions of the images are 200km square.**

## 6 Testing and Results

In order to determine the efficacy of the proposed technique in providing accurate rainfall accumulation values at ground level, a comparison was carried out between raingauge and radar accumulation values for selected rain events; care was taken to compute values which were comparable at ground level. The data from 1996 from the Liebenbergsvlei catchment near Bethlehem were selected as the test for this study. This was because there was a dense network of 45 tipping bucket raingauges placed in a grid, evenly spaced at approximately 10km throughout the catchment at that time (since decommissioned). The Bethelehem S-band radar is also situated in close proximity to the catchment. Both of these factors are important in ensuring accurate estimates of rainfall accumulation values.

The radar rainfall estimates at ground level are estimated in 1km by 1km cells and the raingauge provides a point estimate at ground level. In order to provide an appropriate way of comparing the two estimates, the following approach was taken. The average value of the 9 radar pixels (a 3km square area) centred over a gauge was taken as the radar estimate of average rainfall at each gauge location. In computing the radar accumulation values one needs to take into account that the images are sampled at five-minute intervals, so a simple linear accumulation of the images may not provide an accurate accumulation, especially for fast moving rain events. The accumulations are therefore computed by a Morphing Algorithm that takes into account the motion of the rainfield between instantaneous images (Sinclair and Pegram, 2003).

Block Kriging was used to determine the average rainfall over the same 9km$^2$ area by using all rainguages within a range of 2 correlation lengths from the centre of the 9km$^2$ area, at times corresponding to the radar estimates. The Block Kriging estimates are computed by Equation (6).

$$\hat{z}_D = \frac{1}{D}\int_D Z(x)\cdot dx \tag{6}$$

Where $\hat{z}_D$ is the average value over a selected region and $D$ defines the region (Bras and Rodriguez-Iturbe, 1985: 402-404).

### 6.1 Statistical Comparison of Rainguage and Radar Accumulations

In order to determine the quality of the radar estimates at ground level a statistical comparison of the rainguage and radar accumulations over different periods of 24 hours, 12 hours and 6 hours was conducted. A scatter plot of the radar and rainguage accumulations was done and the correlation coefficient computed. The Kolmogrov-Smirnov test was also used to determine if the cumulative distributions of the radar and rainguage accumulations were significantly different at a significance level of 5%, where the hypothesis being tested is $H_0$: Raingauge Distribution = Radar Distribution against $H_1$: Raingauge Distribution ≠ Radar Distribution. The means and standard deviations ($\sigma^2$) of the accumulated values were also tested at a significance level of 5%.

### 6.2 Rainfall Event Descriptions

Two rain events were selected which contained different rainfall types. The first rain event contained severe convective rainfall in the late afternoon and evening of the 24 January 1996. The analysis for this event was conducted over a 12-hour period from 12:00 to 24:00. The second rain event on the 13 February 1996 consisted of a combination of convective and stratiform rain. The rainfall initially consisted of light stratiform rainfall but towards the evening and afternoon convective rainfall was experienced. The accumulations for the two rain events are indicated in Figure 9. Also indicated on Figure 9 is an approximate outline of the catchment area as well as the rainguage locations. The region directly above the radar, a circle of 20km radius, has also not been infilled due to poor data quality close to the radar during this time period; two raingauges within this region were excluded from the study.

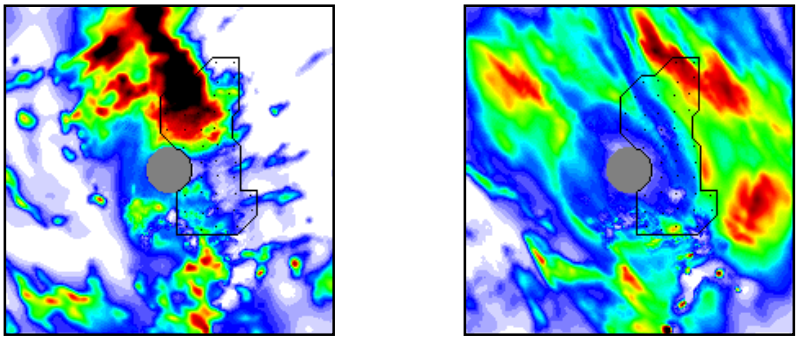

**Rain Event 1: 24 January 1996** **Rain Event 2: 13 February 1996**

**Figure 9. 12-hour and 24 hour rainfall accumulation from the Bethlehem radar on the 24 January 1996 and 13 February 1996. A rough outline of the test catchment is indicated on the image as well as the rainguage locations. Dimensions of the image are 200km square.**

There is a high correspondence for both rain events between radar and rainguage accumulations with an $r^2$ value of 0.86 being returned for the rain event on the 24 January 1996 and an $r^2$ value of 0.78 being returned for the rain event on the 13 February 1996. The highest pair of radar observations bias what is otherwise an excellent fit, and also affects both of the scatter plots in Figure 10. This is probably due to under estimation of the highly localised convective rainfall by the gauges concerned (Wilson and Brandes, 1979).

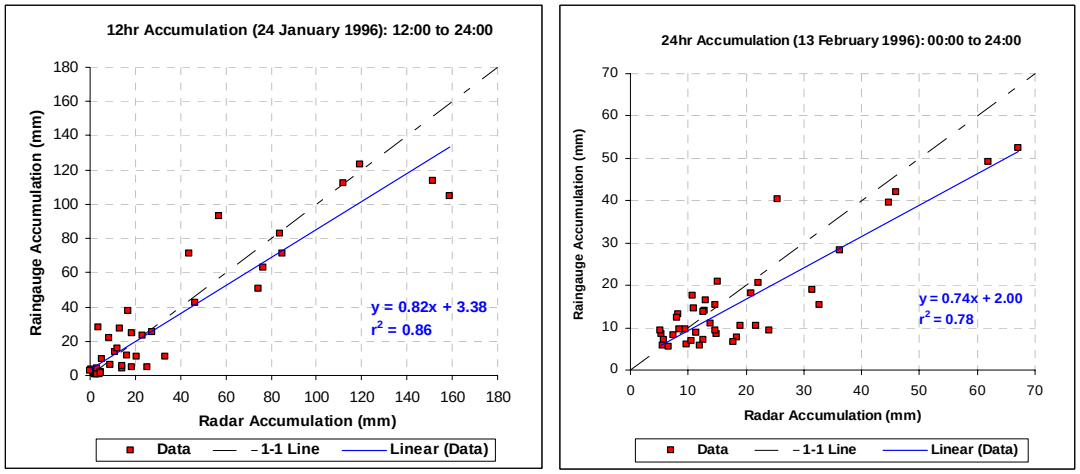


**Figure 10. Scatter plot of radar and rainguage accumulations for a 12-hour accumulation period for the 24 January 1996 rain event and 24 hour accumulation for the 13 February 1996 rain event. A strong correspondence exists between the radar and rainguage accumulation, especially for the high intensity rainfall.**

For the first rain event (24 January 1996) Table 3 provides a summary of the statistical results returned for the rainguage and radar accumulation over a 12 hour period and two 6 hour periods. For the 6 hour period (18:00 to 24:00) and the 12 hour accumulation period there is a close correspondence between the radar and raingauge estimates. With the exception of one standard deviation, the means and standard deviations are statistically similar with the Kolmogrov-Smirnov test (K-S test) also indicating that the distributions of the accumulations for the radar and raingauge are not dissimilar, except for the 6 hour accumulation period from 12:00 to 18:00. The word "Accept" in Table 3 refers to the null hypothesis $H_0$ being accepted and $H_1$ rejected, and "Reject" refers to $H_0$ being rejected and $H_1$ accepted.

**Table 3: Summary of statistical results for different accumulation periods for 24 January 1996 rain event for radar and raingauge data.**

| | 12hr accumulation (12:00 to 24:00) | | 6 hr accumulation (12:00 to 18:00) | | 6 hr accumulation (18:00 to 24:00) | |
|---|---|---|---|---|---|---|
| | **Mean** | **Stdev** | **Mean** | **Stdev** | **Mean** | **Stdev** |
| **Radar** | 30.3 | 41.3 | 4.6 | 5.1 | 27.2 | 40.8 |
| **Raingauge** | 29.4 | 36.8 | 4.0 | 7.1 | 25.4 | 38.3 |
| **Accept / Reject $H_0$** | Accept | Accept | Accept | Reject | Accept | Accept |
| **$r^2$** | 0.86 | | 0.08 | | 0.88 | |
| **K-S TEST** | Accept | | Reject | | Accept | |

For the second rain event (13 February 1996) Table 4 provides a summary of the statistical analysis of the comparisons between rainguages and radar accumulation for the full 24 hour period and two 12 hour periods. The mean and standard deviations for each of the accumulation periods closely correspond and are statistically similar, except for the mean value of the 24 hour accumulation which is probably due to rainguages underestimating the two highest rainfall values. The correlation coefficient value, $r^2$, is also high except for the accumulation period from 12:00 to 18:00 which consisted of light stratiform rain. The cumulative distribution of accumulation values for each time period was also determined to be statistically similar via the K-S test.

**Table 4: Summary of statistical results for different accumulation periods for 13 February 1996 rain event for radar and raingauge data.**

| | 24hr accumulation (12:00 to 24:00) | | 12 hr accumulation (12:00 to 18:00) | | 12 hr accumulation (18:00 to 24:00) | |
|---|---|---|---|---|---|---|
| | **Mean** | **Stdev** | **Mean** | **Stdev** | **Mean** | **Stdev** |
| **Radar** | 18.1 | 14.7 | 1.1 | 1.4 | 17.0 | 14.5 |
| **Raingauge** | 15.8 | 12.2 | 1.0 | 1.5 | 14.8 | 11.9 |
| **Accept / Reject $H_0$** | Reject | Accept | Accept | Accept | Accept | Accept |
| **$r^2$** | 0.78 | | 0.14 | | 0.76 | |
| **K-S TEST** | Accept | | Accept | | Accept | |

## 7 Conclusion

A technique has been presented that extrapolates radar volume scan data estimated at 1km intervals above ground level to the earth's surface, and in the process estimates missing data in the CAPPI stack.

A rainfall classification was firstly done to separate the rainfall into stratiform and convective types. By separating the rainfall, climatological semivariograms for each rainfall type were defined, a procedure which ensures high computational efficiency with little loss in accuracy. The 2km CAPPI level is then examined to determine if a bright band is present and if so the pixels are adjusted on an individual basis. Both 3D Universal and Ordinary Cascade Kriging were then used to infill missing data in the CAPPI stack and finally provide a rainfall estimate at the ground level. In the Kriging computations care was taken to ensure computational efficiency and stability.

The effectiveness of the above algorithm was tested on two different rainfall events exhibiting distinctly different types of rainfall by comparing raingauge and radar accumulation estimates at ground level. The technique demonstrated that the rainfall at the ground from the radar images satisfactorily capture the amount and variability of the rainfall. The conclusion is that the methodology suggested in this article is operationally sound.

## References


Bras, R.L. and Rodriguez-Iturbe, I. 1985. Random Functions and Hydrology. Addison-Wesley Publishing Company. Ontario.

Chiles, J.P. and Delfiner, P. 1999. Geostatistics - Modeling Spatial Uncertainty. Wiley, New York, USA.

Cressie, N. 1993. Statistics for Spatial Data. Wiley-Interscience Publication. New York, USA.

Cressie, N. and Hawkins, D.M. 1980. Robust Estimation of the Variogram, 1. Journal of the International Association for Mathematical Geology. 12, 115-125.

Gordon, A.D. 1981. Classification: Methods for the exploratory analysis of multivariate data. Chapman and Hall. New York, USA.

Jordan, P., Seed, A. and Austin, G. 2000. Sampling errors in radar estimates of rainfall. Journal of Geophysical Research. Vol. 105, No. D2, 2247-2257.

Journel, A.G. and Huijbrechts, Ch. J. 1978. Mining Geostatistics. Academic Press. London, UK.

Marshall J. S. and Palmer W. M. 1948. The distribution of raindrops with size, Journal of Meteorology. 5, 165-166.

Matheron, G. 1962. Traite de Geostatistique Appliquee, Tome I. Memories du Bureau de Recherches Geologiques et Minieres. No. 14. Editions Technip, Paris.

Mittermaier, M.P., 1999. Investigating the Characteristics of the Radar Reflectivity Profile. MSc Eng dissertation, Civil Engineering, University of KwaZulu-Natal, Durban, Howard College.

Sabyasachi, B., Gunst, R.F., Guertal, E.A. and Hartfield, M.I. 1987. The Effects of Influential Observations on Sample Semivariograms. Journal of agriculture, biological, and environmental statistics. 2, 490-512.

Sanchez-Diezma, R., Zawadzki, I. and Sempere-Torres, D. 2000. Identification of the bright band through the analysis of volumetric radar data. Journal of Geophysical Research. Vol. 105, N0. D2, 2225 – 2236.

Sinclair, D.S. and Pegram, G.G.S. 2003. Combining traditional and remote sensing techniques of rainfall measurement as a tool for Hydrology, Agriculture and Water Resources Management. Proceedings 11th SA National Hydrology Symposium, Port Elizabeth, South Africa.

Steiner, M., Houze, R.A., Yuter, S.E. 1995. Climatological Characterization of Three-Dimensional Storm Structure from Operational Radar and Rain Gauge Data. Journal of Applied Meteorology. 34, 1978 – 2007.

Terblanche, D.E., Pegram, G.G.S., Mittermaier, M.P. 2001. The development of weather radar as a research and operational tool for hydrology in South Africa. Journal of Hydrology. 241, 3 – 25.

Wesson, S.M. and Pegram, G.G.S. 2004. Radar rainfall image repair techniques. Hydrology and Earth System Sciences. 8(2), 220 - 234.

Wilson J.W. and Brandes E.A. 1979. Radar measurement of rainfall – A summary, Bulletin of the American Meteorological Society. 60(9), 1048-1058.